Monte Carlo Simulation of Diffusion MRI in geometries constructed from two-photon microscopy of cortical gray matter

Nima Gilani[1], PhD, Sven Hildebrand[1], MSc. (microscopy), Anna Schueth[1], PhD, (microscopy), Alard Roebroeck[1], PhD

[1] Department of Cognitive Neuroscience,

Maastricht Brain Imaging Centre (MBIC),

Faculty of Psychology & Neuroscience,

Maastricht University

Corresponding author: Alard Roebroeck, PhD,

Department of Cognitive Neuroscience,

Maastricht Brain Imaging Centre (MBIC),

Faculty of Psychology & Neuroscience, Maastricht University

Postal address: PO Box 616, 6200MD, Maastricht, the Netherlands

a.roebroeck@maastrichtuniversity.nl

Running title:

Simulation of Diffusion in the Cortex

Abstract

Purpose: Diffusion MRI of the cortical gray matter has shown to be sensitive to diseases such as Alzheimer's disease and multiple sclerosis. Additionally, there is a growing interest in remodelling, characterization and improvement of the understanding of different brain areas using a combination of quantitative MRI or 3D microscopy. The purpose of this study was to quantitatively characterize the cytoarchitecture of cortical tissue from fluorescence microscopy in order to simulate diffusion in the cortex and to better understand its diffusion signal characteristics

Methods: Cellular volume fractions, and sizes of glial nuclei, and neurons were measured from 3D microscopy by volume segmentation and non-linear least squares ellipsoid fitting. Diffusion of water molecules in the cortex was simulated for variable permeability levels, free diffusion coefficients, cell (neuron, glia, dendrite or axon) densities, and sizes and diffusion times. Some parameters such as axonal density were extracted from the available literature. In an alternative method, the simulation geometry was directly extracted from available microscopy data of the cortex. The simulations were compared with fractional anisotropy, apparent diffusion and kurtosis values reported *in vivo* in the healthy brain.

Results: Assuming a permeability of around 20-30 μms^{-1} and a free diffusion coefficient of around 1.6-1.7 $\mu m^2 ms^{-1}$, the simulated fractional anisotropy, diffusion coefficient and kurtosis of the cortical gray matter were on average around 0.2-0.4, 0.7-1.3 $\mu m^2 ms^{-1}$, and 0.1-1.0, respectively, which are in ranges in agreement with previous *in vivo* reports.

Conclusions: The Monte Carlo simulations of different layers or areas of the healthy cortex, and extrapolation of these simulations to other cell sizes or densities is an additional step in better quantitative characterization or remodelling of the healthy or diseased cortex from diffusion MRI.

Keywords: Cortical gray matter, Monte Carlo, Neurons, Diffusion MRI, Glial cells, Axon

Introduction

Variations in tissue micro-structure of the cortex have been observed for diseases such as schizophrenia [1, 2], Alzheimer's disease (AD) [3-5], and Huntington's disease [4] in addition to age-related changes [6]. Diffusion MRI has been a successful and commonly used imaging modality to differentiate or characterize different diseases in the last decades [7] because of its ability to give estimates of tissue micro-architecture [8, 9].

It has been hypothesized that changes in cortical microstructure (e.g. cell density or sizes and demyelination) result in observable variations in parameters derived from diffusion-weighted or tensor imaging (e.g. fractional anistropy or mean diffusivity) [10-12]. Kroenke C. D. [10] introduces a number of references where variations of FA have been of interest to study maturation of the cortex. Vrenken et al. [11] have shown that there might significant decreases in FA of the cortex for patients with multiple sclerosis (MS). Microstructural changes associated with AD are decreased dendritic arborization, loss of synapses or dendritic spines [13-16] and selective loss of neurons [5, 17, 18]. Parker et al. have shown that these changes might result in decreases in orientation dispersion and neurite density indices (ODI/NDI) derived from neurite orientation dispersion and density imaging (NODDI) [12].

In addition, it is important to use diffusion MRI derived parameters or quantitative 3D microscopy to further model or improve our understanding of the cortical gray matter. Recently, Ganepola et al. [19] proposed the use of diffusion MRI derived parameters to redefine the widely used Brodmann’s areas [20] of the brain. Also, Bastiani et al. hypothesized with improvements in SNR’s of diffusion MRI it might be possible to delineate the borders of layers of the cerebral cortex [21].

Cortical matter is a dense composition (i.e. an around 84% volume fraction) of axons, neurons, dendrites, glial cells, and blood vessels [22]. Despite this high level of cellularity, apparent diffusion coefficients measured from the cortex are relatively high compared to the white matter. This could be explained by: a) the relatively large sizes of neurons (generally greater than 20 µm [2, 23, 24]) and b) glial minimum diameters of at least 2.5-3 µm [25], compared to very thin axons in the white matter with diameters of generally less than 1 µm.

Layered composition of the cortical matter and its voxel level mixture at borders with cerebro-spinal fluids (CSF), and WM which have their distinct diffusion characteristics, supposedly results in the diffusion signal to be multi-exponential. Initially Maier et al. [26]

proposed the use of biexponentials describing diffusion in cortical voxels adjacent to the white matter or CSF. The more evolved notation of compartmental diffusion, NODDI [27], has recently become a candidate for analyzing diffusion in the cortex [28, 29].

Moreover, there are numerous reports of quantitative diffusion MRI of the cortical gray matter in recent years [1, 11, 12, 26, 28, 30-32]. However, diffusion MRI of the gray matter has received relatively less attention compared to white matter for two reasons. First, cortical gray matter has a relatively smaller anisotropy, and hence less measurable changes in fractional anisotropy for different diseases. Secondly, Monte Carlo simulations of diffusion have indicated the high sensitivity of diffusion-weighted derived parameters ADC and kurtosis to permeability levels [33]. Hence, there are less mydelination de-myelination related variations of the diffusion signal in cortical gray matter compared to white matter.

Immunohistochemistry [5], scanning electron microscopy [34], different light microscopy techniques [35] such as two-photon microscopy [36], and ultra-high field (UHF) diffusion MRI [37] of *ex vivo* tissue samples have improved our understanding of the cortex micro-structure in the last years. However, since there are a number of morphological changes in the fixation process [33, 38, 39] in addition to temperature differences, extrapoloation from *ex vivo* MRI or microscopy to analysis *in vivo* diffusion MRI require conservative mathematical modellings.

Here, Monte Carlo simulations of diffusion similar to the ones already performed for white matter [40-42], and prostate [33, 43] were employed to further study diffusion MRI of the cortex. Initially, residence times of water molecules in layered structures mimicking cortical matter boundaries were measured from Monte Carlo simulations. Residence times of water molecules inside small voxels that might be affected by boundary effects near the cortical matter were also measured. Knowledge of these residence times was helpful in estimating how much a voxel within a layer was representing that physical layer and was not affected by boundary effects in addition to derivation of minimum voxel sizes for *ex vivo* MRI. Later, diffusion MRI was simulated in the cortical matter using two different approaches: geometrical reconstruction of cell bodies, and direct simulations from microscopy). For both of these simulation methods, microstructural parameters were either measured from light microscopy or were directly used from the literature. Simulation were performed for different cell compositions mimicking different cortical layers. Additionally, simulation results were

compared and cross validated with their available *in vivo* measurements in published literature listed below.

Materials and Methods

Residence times of diffusion layers

We aimed at considering and simulating diffusion within different coritical layers characterized by their axon, neuron, dendrite, or glial composition, in addition to myelination of axons, or variations in cell sizes. Layered diffusion measurements such as the ones by Mukern's team [26] and the ones using NODDI [12, 28] are highly affected by boundary effects or simultaneously having CSF and GM, or GM and WM in a single voxel *in vivo*. This issue is less significant for *ex vivo* measurements because of higher resolutions. Hence, NODDI has been used to separate myelo- and cyto-structural cortex layers [29]. However, there might be high exchange of spins between layers, and each voxel might be an average of a neighbourhood of voxels. Diffusion compartments or layers give their characteristic diffusion signal only if they have a negligible exchange with their neighbouring compartments or residence times within each compartment are long compared to acquisition times (echo time in diffusion or T2, or TI in T1 weighted imaging) [43]. Residence times is the inverse of exchange rates and could be used alternatively.

There are two different scenarios where the concept of residence time could help in feasibility assessment of separating physical diffusion compartments. The first case is having multiple microstructural compartments (each of them with their distinct diffusion characteristics) within each voxel; in this case low exchange between the compartments allows multi-exponential fitting on the diffusion signal (e.g. [33] for the prostate, or [26, 27] for the brain). The second case is when the purpose is to check how much a voxel characterizing a microstructural layer is affected by nearby layers or neighbouring voxels.

The concept of residence times could also be used for T2, T1 relaxometry purposes. For example, T1 and T2 signals of the knee cartilage have shown to be multi-exponential in the knee cartilage because two tightly and loosely bound macromolecular water molecules are present there, or two distinct T2 compartments (ductal lumen and the cellular tissue) have been observed in the prostate [43, 44]. In all of these cases, longer residence times of water molecules in each compartment relative to acquisition times result in better separation of compartments.

Here, residence times were measured for 3 different scenarios: one plate (mimicking the WM, GM boundary), two plates (mimicking cortical laminar structure), and six plates (mimicking a voxel).

One plate

Three-dimensional random walk simulation was performed in a geometry consisting of two compartments separated by an infinite plane (Fig. 1 a). The purpose was to show how long the water molecules at each initial position reside in the medium A compared to the acquisition time dependent on their initial position. Initial position of water molecules was normalized to $\sqrt{Dt}$ (where D was diffusion in the comparmtent and t was the acquisition time) and residence times were normalized to acqisition times. This normalization allowed for generalization of the simulation to any other similar geometry. However, here we interpreted the results for a specific case of white matter, and grey matter boundary.

Two plates

Three-dimensional random walk was performed in a geometry consisting of three compartments (medium) separated by two infinite planes (Fig. 1 c). The purpose was to determine residence time of water molecules in the central compartment relative to acquisition times for different initial positions. Later, results were normalized similar to the one plate simulation. While the results could be used for interpreting diffusion in any layered diffusion compartment, here the purpose of the simulation was to investigate residence times in the layered structure of the cortical matter.

Six plates (voxel)

Similar to the one, and two plate simulations, a simulation medium consisting of a voxel surrounded by 6 plates (Fig, 1 e) cutting a cubic voxel was designed. Residence times of water molecules in the voxel were measured for different initial positions of spins in the voxel. This simulation could give a limit for how much we could decrease voxel sizes in a specific tissue, for different acquisition times without the voxel being affected by the neighbouring voxels.

Microstructural parameters derived from literature

There are numerous measurements of neuronal, glial, blood, or axonal cell sizes, cell densities or cell volume fractions in the healthy or diseased brain. Azevedo et al. [45] have found that there are around 86.1 billion neuronal and 84.6 non-neuronal cells in the human

brain. The neural parenchyma is mostly made of neurons and glial cells and less than 3% its volume is made of vasculature [46], hence most of these non-neuronal cells could be assumed to be glial cells [47]; glial cells are various astrocyte types, oligodendrocytes, microglial and various precursors cells. Additionally, it has been shown that with increasing neuron diameters, glial/neuronal ratio increases; this has been hypothesized to be because of the increased metabolic needs of larger neurons [47, 48]. Accordingly, it has been hypothesized glial/neuronal volume ratio might be of more interest to neuroscientists compared to glial/neuronal cell count [47]; this paradigm shift in cell measurements might benefit diffusion-weighted MRI analysis because diffusion parameters have been shown to highly rely on and have been described vs. cell volumes and volume fractions [33, 43, 49].

There are two main types of neurons in the cortex: pyramidal cells with diameters ranging from 20 to 120 µm, and granule cells which are star-shaped, have short axons, make local connections, and their diameters are around typically less than 20 µm [50]. The average area of pyramidal neurons (soma) in the healthy human posterior hippocampus have been measured to be 559±17.8, 552.2±31.2, 596.5±39.9, and 581.7±26.3 μm^2 for cornu ammonis (CA) sub-regions of 1 to 4, respectively [2]. Jönsson et al. [23] have measured areas of 353.4±31.6, 415.0±88.9, 457.4±115.9, and 523.5±106.9 μm^2 for the neurons for CA 1 to 4, respectively. Additionally, the neuronal soma sizes are measured to be 11.8±0.4, 15.5±0.4, 12.4 ±0.4, 15.7±0.4, 15.7±0.5 in layers II, III, IV, V, VI of the prefrontal cortex of healthy subjects in reference [25]. Cotter et al. [24] have measured neuronal areas in the healthy human anterior cingulate cortex (ACC) to be around 106, 263, 493, 737, 804, and 741 μm^2 for cortical layers 1 to 6, respectively. In a more recent reference [51] using fluorescence microscopy the corresponding neuronal areas were measured to be 182-265, and 166-187 μm^2 for Brodmann areas 24, and 47, respectively.

Average values of axonal diameters in the human cortical white have measured to be 0.63 to 1.34 µm (range of 0.19 to 4.79 µm) [52]. Additionally, Liu and Schumann [53] have measured average diameters of 0.8-0.85 µm for the white matter beneath the superior temporal cortex using electron microscopy. Zikopoulos and Barbas [54] have measured axonal diameters of 0.5-0.6 µm for the white matter beneath the lateral frontal cortex. Accordingly, three axonal diameters of 0.6, 1, 2 µm were used for simulation purposes in this study.

Deitcher et al. [55] have measured average dendritic lengths and diameters of 540-800 µm (dependent on depth from pia) and 0.76 ± 0.28 µm, respectively, in HL2/L3 of human neocortex.

Microscopy measurements

Cortex geometry was reconstructed for simulation purposes using two-photon microscopy. The parameters of interest such as neuronal or glial cell radius, and volume fraction estimated from three-dimensional two-photon microscopy (TPM) data of [56].

A filtering and Otsu thresholding based algorithm was developed in order to measure glial nuclei (v_g), and neuron volume fractions (v_n) using RGB images available of a Nissl-like fluorescent cell-body lebel [56]. Accordingly, extracellular volune fraction (v_e) was approximated as (1- v_n - v_g) assuming there are no other significant barriers for diffusion of water molecules.

The neuronal diameters are generally in ranges of 11-27 µm (mostly around 20-25 µm) as discussed above. However, there are two issues that need to be addressed: first, pyramidal neurons have been assumed spherical in order to estimate their diameters. Second, the areas have been measured using two-dimensional images and such estimates of diameters are always an underestimation of cell sizes. Instead, there are a number of methods to recover 3D shapes of cells which are mentioned in [57]. Alternatively, high resolution and three-dimensional two-photon microscopy acquisitions of the brain cortex could be employed to estimate neuron and glial cell sizes.

A non-linear least squares based ellipsoid fitting function [58] was used in MATLAB Release 2017a (The MathWorks, Natick, Massachusetts) to characterize and estimate radii of neurons and glial cells separately. The function required at least 9 perimeter points to fit an ellipsoid; however, this condition was not adequate and an additional condition of having the points spread in at least 3 parallel planes was taken into account. Voxels corresponding to areas of glial nuclei and neurons in the visual cortex were segmented separately, and ellipsoids were fitted on them. Fig. 2 (a), and (b) are segmented areas of a neuron and a glial cell, respectively. (maybe add the fit as well)

v_n , and v_g ranges were 0.12-0.35, and 0.03-0.13, respectively, in 10 different TPM slides. The glial nuclei on average could be described as ellipsoids with the longer radii of 8.98±1.77 (ranging from 6.66 to 11.00) and smaller radii of 2.73±0.63 (ranging from 1.66 to 3.50). However, spheres better fitted on the neurons with average radii of 12.0±4.6 (ranging from 6.1 to 24.7) µm.

Geometry based indirect simulation

Glial, neuronal, or axonal sizes and densities from the previous sections were used as inputs to simulate diffusion MRI in the cortex. Mixtures of ellipsoids and cylinders with variable cell sizes and densities were used as geometry for simulation of diffusion in the cortex. Water molecules were randomly placed within the geometries and randomly moved with time steps of 1-25 µs corresponding to random walk steps of 0.09-0.48 µm assuming free diffusion coefficient of 1.6-1.7 $\mu m^2 ms^{-1}$. Permeability of different geometries was variable and simulated giving random chances of crossing to different permeability levels [33]. Pulsed gradient spin echo (PGSE) acquisition was simulated by recording changes in the phase of these randomly moving spins after the application of the diffusion gradients. Finally, diffusion kurtosis model [59, 60] was fitted on the signal. Detailed equations regarding simulation of random walks, permeability, and PGSE could be found in [33, 43].

Neuronal radii of 10 or 20 µm were considered for all of the simulations. Glial cells were modelled as ellipsoids with radii of 2.7, 2.7, and 9 µm and three different radii of 0.3, 0.5, and 1 µm were considered for the axons. Different cortex areas or layers have different compositions; it is a time-consuming challenge to simulate and summarize all of these compositions in a single manuscript. Hence, here three different and simplified geometry scenarios which were mostlikely to simulate the visual cortex were considered.

The first scenario was the simulation of neurons and glial cells with varied neuron size and densities. Neuron volume fractions of around 0.1, 0.2, 0.3, and neuronal diameters of 10, and 20 µm were considered. This scenario mostly corresponds to layers II or III of the cortex.

The second scenario was simulations of myelinated or unmyelinated axons with diameters of 0.6, 1, 2 µm and volume fractions of 0.1, 0.3, 0.6, 0.9; where for axonal volume fraction of 0.9 hexagonal circle packing was employed and the other fractions were made by expanding the geometry phase space while keeping axonal morphology constant. It has been proven that hexagonal circle packing leads to the maximum possible volume fraction which is 0.9069 [61]. This simulation corresponds to layer six of the cortex, or in general white matter

beneath the cortex. Permeability values of 10 and 30 μms^{-1} were considered corresponding to myelinated and unmyelinated axons, respectively.

The third scenario consisted of the mixtures of the two scenarios above. Neuronal and glial volume fractions were kept constant at 0.1, 0.05, respectively. Axonal volume fractions for this mixture varied between 0 to 0.3. This scenario mimics layers IV and V of the cortex.

For all of the simulations, 15 equally distanced *b*-values ranging between 0 to 2500 smm^{-2} were used. Four different diffusion times of 40, 60, 80, and 100 ms were used; definition of diffusion times was similar to [33, 38, 43]. Two D_{free} (defined in [33, 38, 43]) values of 1.6, and 1.7 $\mu m^2 ms^{-1}$ were used for the simulations which have shown to be consistent with *in vivo* measurement of free diffusion which is affected by protein solutions [33]. The values could also be verified by ADC estimates of 1.6-1.9 $\mu m^2 ms^{-1}$ parallel to the direction of axons in reference [62], where these values are from a diverse range of 1.5-3 T Philips or Siemens scanners; note that diffusion parallel to the direction of fibre bundles in nearly free because axonal lengths are generally around or greater than a few hundreds of micrometres. Additionally, these are all in agreement with consideration of an inherent D_{free} of 1.7 $\mu m^2 ms^{-1}$ in NODDI algorithms [27, 28].

Direct simulation from microscopy

The ideal scenario for Monte Carlo simulation of diffusion is to directly use the geometry from microscopy in comparison with the mathematically reconstructed geometries of the previous section. This has been the subject of a recent study by Palombo et al. [63], where they have directly segmented area of cells from microscopy and simulated the random walks of thousands of spins within these geometries. However, the main issue with this approach is the long simulation times which will linearly increase with increasing of cell numbers, and the complexity of their area segmentations.

Additionally, a two-dimensional version of such direct simulation has been presented in [64] where only one cell type has been considered. However, they have not mentioned how three-dimensional simulation mediums have been constructed from two-dimensional images (a recent reference [57] extensively discusses how this might be a formidable challenge).

Alternatively, here we used Matlab's colour-based volume segmentation to separate different cell types or giving them regions numbers in two-photon microscopy samples. The region number was ascribed to each voxel based on its cell type or being in the extracellular space.

Diffusion of water molecules was simulated within each voxel and if for each of the random walks the spin travelled to a neighbouring voxel with different geometry type, the available algorithm for permeability explained in the previous section was used to allow or reflect the random walk. Similar to [63], this method enabled different permeability ascriptions to each cell. Using this simplistic algorithm, random walk simulation of millions of spins took only a few hours on an Intel Xeon 3.60 GHz processor and there were not any requirements for complex reconstruction of biological geometries.

We tested this method on three dimensional two photon microsopy samples of the visual cortex already used for publication in [56]. The acquistion details were: number of slices 21, slice thickness 4.98 µm, FOV 369.40×369.40 μm^2, and matrix 1024×1024.

Optimal acquisition and modelling

A number of different factors should be considered when selecting *b*-values in a simulation or in a real acquisition. Some of these factors are the maximum *b*-values [65] and the corresponding systematic biases in diffusion estimates, and the optimized set of *b*-value in order to increase parameter estimations [66]. For example, if the purpose of the acquisition is to count cells, measure densities, or estimate cell type fractions, more specific *b*-value optimizations could be performed. Palombo et al. [67] have shown that the Stick model for diffusion is more sensitive to radii of soma at low *b*-value regimes (1-3 $ms\mu m^{-2}$), whereas, for a constant soma radius of 5 µm and ultra high *b*-values (3-15 $ms\mu m^{-2}$), the volume fraction of soma is more effective on the signal. First, they considered only small soma radii of 5 µm and have only used Stick model, without considering other models such as kurtosis. Second, it is recommended to optimize models and acquisition protocols after having sets of in vivo or ex vivo maps coregistered with microscopy in order to optimize estimation of certain microstructural parameters instead of using Monte Carlo simulations. Third, for the cortex cell mixture where different cells types are close to each other and residence times of water molecules in each of these cell type compartments is low, giving specific details about cell sizes and fractions seem to be nearly formidable. The contrary example is the prostate cell mixture where water molecules reside in ducts for long times [43] and the use of multi-compartmental or multi-exponential models is allowed.

Results

Geometry based diffusion simulation results

Figure 3 is a plot of D and K derived from simulation of the mixture of neurons, and glial cells mimicking layers II, and III of the visual cortex. The indirect simulation method was used to reconstruct this geometry. For ADC, over diffusion times there is a near uniform ADC decrease for decreasing cell size and for increasing cell density (neuronal volume fraction, NVF). K better distinguishes cell sizes, especially for long diffusion times, where K increases with decreasing cell size. K better distinguishes cell sizes, especially for long diffusion times, where K increases with decreasing cell size. For small size sizes, K increases for increasing cell density/NVF. However, there I no such effect for the bigger cell sizes. Explain in term of K as the difference in D between 2 compartments.However, there was not a monotonic trend of changes in kurtosis. This was expected for two reasons: first because of the unpredictable nature of kurtosis from Kärger-Jensen [59, 60, 68] two compartmental equations, and second because of very low precision in the estimation of parameter kurtosis due to its dependency on *b*-values [65, 66].

ADC of myelinated or unmyelinated axons with different cell sizes or volume fractions close to deep layers of the cortex are shown in Fig. 4. Obviously, there are decreases in ADC with increasing myelination (decreasing permeability), and increasing axon radii. However, there are no monotonic changes in ADC with changes in axonal volume fractions. For sparse axon densities (less than 30%), with increasing cell density ADC decreases, whereas, for highly packed cells this monotonic behaviour is not observed. Again this could be predicted from Kärger-Jensen [59, 60, 68] equations, considering the fact that for highly packed axons the extra-cellular ADC is relatively smaller that intra-cellular diffusion. Additionally, it was noticed that variations of diffusion parameters over different diffusion times were small. This is because radii of axons are small and such differentiation could be improved only by using ultra-short diffusion times are generally infeasible for clinical studies.

It was observed that nearly all of the anisotropy in the cortex is caused by axons/dendrites and other cell structures such as neurons or glia have a negligible effect on anisotropy. However, this argument would not rule out that an anisotropic pattern of neuronal cells might have substantial impacts on the measured fractional anisotropy.

Direct diffusion MRI simulation from microscopy

Fig. 5 is the measured ADC and K from the direct diffusion simulation in the abovely mentioned two-photon microscopy sample. These values are in agreement with the simulations of Fig. 2 which could be approximately ascribed to geometries of layers II, and III.

Comparison with *in vivo* MRI

There are several reports of parameters derived from diffusion-weighted imaging in the cortical gray matter *in vivo*, some of which are summarized in table 1. These values are in a broad agreement with the simulations results.

Optimal *b*-values or diffusion times for estimating cortex microstructure

It is obvious from Fig. 2 that higher diffusion times might help in better estimating neuronal cell sizes in pure neuronal voxels. However, distinguishment of their volume fractions is low regardless of diffusion times. Considering that apparent diffusion and kurtosis values are around 1-1.4 $\mu m^2 ms^{-1}$ and 0.3-0.8, respectively, the use of low *b*-values are recommended to decrease biases in estimating time-dependent diffusion and kurtosis. This is in agreement with the recommendations of references [65, 69].

In case of pure axons (Fig. 3), shifting diffusion times in clinically feasible ranges for *in vivo* acquisitions might not help in giving better estimates, however, for *ex vivo* acquisitions there might be possibilities of using short diffusion times of less than 20 ms to improve axonal volume fractions and radii. In this case, medium to high *b*-value regimes might give better estimates of the axonal microstructure.

In mixtures containing different cell types, the argument seems to be the same, the choice of b-value should be based on the purpose of study. If the aim is to characterize layers with different axon compositions, then short diffusion times might give better estimates of myelo-structure. However again maximum *b*-values should be chosen considering average diffusion and kurtosis values not to have too many biases in estimations [65]. Additionally, care should be taken not to too much extrapolate to tissue microstructure.

Based on the results presented about residence times in different layers, decreasing diffusion times would also help in better distinguishing cortex layers. Hence, the recommended choice of diffusion times and *b*-values could be variable for the purpose of each study.

Discussion

Simplified diffusion simulations in mathematically reconstructed geometries, or alternatively the novel direct simulations from microscopy might help in better microstructural characterization of diseases such as Alzheimer's, Parkinson, etc. Monte Carlo simulation of diffusion in these reconstructed geometries would help in improving our understanding of the physics of diffusion in each tissue type, and to more firmly reject or further confirm many of the existing models [70, 71]. Additionally, direct simulation of diffusion in different cortical areas if averaged for many samples would enable the creation of a library of direct diffusion simulation in the brain.

Fig. 3 is in agreement with previous studies [72, 73] stating that time-dependent diffusion measurements of axons with diameters of around 1 μm are sensitive to diffusion time at very short diffusion times (around a few milliseconds), whereas, for typically longer *in vivo* diffusion times of 40-100 ms changes in diffusion parameters vs. diffusion time are negligible. The same applies to simulations of gray matter [72]; however, at diffusion times of 40-60 ms more substantial variations in diffusion parameters relative to microstructural variations are observed compared to white matter. This might imply that considering the limits of clinical scanners, time-dependent diffusion measurements might more feasibly enable characterization of gray matter compared to white matter.

The results here further validate some of the commonly accepted arguments about correlations between microstructural changes and diffusion-weighted MRI observations. The examples are increases in permeability of axons (demyelination), increases in cell sizes (with constant cell density and structure), and increases in the heterogeneity of the mixtureincreases in the heterogeneity of the mixture which result in decreases in fractional anisotropy, increases in ADC, and increases in kurtosis, respectively [43, 59, 60]. However, these simulations do not serve as proof but cross-validation for such statements. Hence, care should always be taken when the aim is to estimate microstructural parameters from diffusion-weighted MRI [74].

It has been discussed in [75] that since there are different cell types in each voxel in addition to intrusions from CSF or WM, extrapolating the parameters derived from dMRI to variations in specific biophysical parameters is somehow more formidable compared to other tissue types such as the brain. For example, FA has a high correlation with myelination in white matter whereas this correlation is very weak for the cortex.

Aggarwal et al. [76] have measured layer specific FA values *ex vivo* for Brodmann areas 4, 9, 17, and 18 and have plotted them versus cortical depths. These plots have relatively small inter-subject variability but are variable for each of these areas. FA values are generally less than 0.2-0.25 in the cortex and are substantially variable for each layer. In addition to the well known compositional effects on FA, they have also raised the possibility that decreases in FA of some layers could be caused by having tangential and radial crossing fibres in a voxel. Creating different perspectives for the cortex by different means such as the creation of gyral coordinate system [77] might also help in discovering more of neglected explanations for variations in diffusion signal.

Additionally, the results presented here challenges one of the widely used statements in diffusion MRI i.e. increases in cell density results in monotonic decreases in diffusion kurtosis. While for sparse or scattered cells (less than 30%) this statement might hold true, for highly packed and myelinated axons this statement is not valid. This finding is in agreement with two compartmental analysis of Jensen et al. [59, 60] which are based on two Kärger model [68] because at very high cell densities the extracellular spaces have a lower diffusion coefficient compared to the intracellular spaces and increases in their volume fraction with minor changes in their ADC in fact results in small reductions in ADC of the total tissue.

It is generally better to make more conservative statements about parameters derived from diffusion-weighted imaging of white matter [74]; this is also applicable to a complex mixture such as the cortex where four different cellular microstructures simultaneously affect the diffusion.

We intend to use the direct microscopy simulation for a variety of microscopy acquisitions in different brain areas and compare the values with their coregistered *ex-vivo* diffusion MRI. Additionally, the works might be extended to microscopy of other tissue types in the body.

Diffusion MR has shown success in better characterization of the laminar mesostructure of the cortex in recent years [29] . We felt that there was a missing step in correlating variations in cortex composition and microstructure with the diffusion signal. More simuultaneous high-resolution MRI and light microscopy data will help in finding these correlations; however, simulations could make them more specific. We did not confirm nor reject specificity of models such as NODDI or Stick model for diffusion. These models could be further investigated for the precision of model fitting either using Cramér-Rao lower bound such as in [66, 78, 79], finding the systematic biases in parameter estimations dependent on

maximum *b*-values [65], missing analysis regarding how separate the compartments (if exchange rates are low) [43], or more in terms of how the models have been derived [70]. Regardless of these complexities, diffusion MR has been successful in distinguishing laminar layers if high resolutions *ex vivo* acquisitions are used. Whether simplistic or more advanced modellings are used, there might be a paradigm shift in future studies to make more microstructurally specific correlations between diffusion parameters and the laminar structure of the cortex

There were a few shortcomings for this work which might be alleviated for the future. First, simultaneous staining axons and neurons, glia, or in general all of the cortical matter microstructure would have been better for direct Monte Carlo simulations. While such staining is feasible for thin layers, it becomes challenging to thick layers of a few hundreds of micrometres which are more helpful for direct Monte Carlo simulations of diffusion.

Second, stimulated echo acquisition mode (STEAM) has recently been found applicable to such genre of studies *in vivo* or *ex vivo* [80, 81]. Simulating STEAM diffusion MRI is not too complex and has been performed in [41]. Additionally, here we aimed at comparing the simulation results with abundantly available *in vivo* instead of *ex vivo* MRI data. This is because there are many differences between *ex vivo* and *in vivo* MRI such as fixation effects, temperature differences, etc. that makes direct extrapolation of *ex vivo* measurements to the analysis of in vivo MRI data a formidable task; this has been discussed for the prostate in [33] and for the brain in [39].

There might be a number of recent works with similar goals, this study however has some improvements such as successful simulation of permeability instead of assuming all micro-structural walls are impermeable compared to [82] or lack of requirement any complex mathematical and time-consuming construction of microstructure such as in [63] and instead direct simulation of microsture from light microscopy data.

Acknowledgements

NG and AR were supported by a Dutch science foundation (NWO) VIDI Grant (#14637). Additionally, AR was supported by an ERC Starting Grant (MULTICONNECT, #639938).

Tables

Table 1. Diffusion-weighted measurements of the cortex from the literature.

Figure Captions

Fig. 1 Residence time simulations in two mediums (WM and GM) separated by one plate (a) and (b), three mediums (cortical layers) separated by two plates (c) and (d), and inside a voxel (e) and (f). Notes: the dashed lines in (b) and (d) are x of the planes. For (b-f) all of the plates were either located at -5.27 or 5.27 $/(Dt_{max})^{0.5}$

Fig. 2 A 3D rendering of the 3D microscopy volume, with nucleus label in blue and cytoplasmic cell body label in green (a). Segmented areas of a neuron (b) and a glia (c) and the ellipsoids fitted to them. On average neurons were best described by spheres with radii of 12.0±4.6 and glia by ellipsoids with axes 2.73±0.63, 2.73±0.63, 8.98±1.77 µm in the visual cortex with N=50. Note: resolution and slice thickness of microscopy were 0.36×0.36 µm2, and 4.98 µm, respectively.

Fig. 3 ADC (a) and kurtosis (b) of the simulated neuronal/glial mixture with variable neuron volume fractions (NVF) and neuron radii (NR), for constant glial volume fraction, for diffusion times of 40-100 ms, with the indirect (first) simulation method. Glial sizes were the same as Fig. 1 and their volume fraction was 0.03-0.07.

Fig. 4 ADC simulated myelinated (a) and unmyelinated (b) axons with variable axonal volume fractions (AXV) and axon radii (r), in absence of cell bodies, for diffusion times of 40-100 ms, with the indirect (first) simulation method.

Fig. 5 Direct simulation of (a) ADC and (b) *K* in a TPM microscopy sample of the visual cortex.

References

1. Seitz, J., Y. Rathi, A. Lyall, O. Pasternak, E.C. del Re, M. Niznikiewicz, P. Nestor, L.J. Seidman, T.L. Petryshen, and R.I. Mesholam-Gately, *Alteration of gray matter microstructure in schizophrenia.* Brain imaging and behavior, 2018. **12**(1): p. 54-63
2. Benes, F.M., I. Sorensen, and E.D. Bird, *Reduced neuronal size in posterior hippocampus of schizophrenic patients*. Schizophrenia bulletin, 1991. **17**(4): p. 597
3. Thompson, P.M., M.S. Mega, R.P. Woods, C.I. Zoumalan, C.J. Lindshield, R.E. Blanton, J. Moussai, C.J. Holmes, J.L. Cummings, and A.W. Toga, *Cortical change in Alzheimer's disease detected with a disease-specific population-based brain atlas.* Cerebral Cortex, 2001. **11**(1): p. 1-16
4. Jernigan, T.L., D.P. Salmon, N. Butters, and J.R. Hesselink, *Cerebral structure on MRI, Part II: Specific changes in Alzheimer's and Huntington's diseases.* Biological psychiatry, 1991. **29**(1): p. 68-81
5. De Calignon, A., M. Polydoro, M. Suárez-Calvet, C. William, D.H. Adamowicz, K.J. Kopeikina, R. Pitstick, N. Sahara, K.H. Ashe, and G.A. Carlson, *Propagation of tau pathology in a model of early Alzheimer's disease.* Neuron, 2012. **73**(4): p. 685-697
6. Jernigan, T.L., S.L. Archibald, M.T. Berhow, E.R. Sowell, D.S. Foster, and J.R. Hesselink, *Cerebral structure on MRI, Part I: Localization of age-related changes*. Biological psychiatry, 1991. **29**(1): p. 55-60
7. Le Bihan, D. and H. Johansen-Berg, *Diffusion MRI at 25: exploring brain tissue structure and function.* Neuroimage, 2012. **61**(2): p. 324-41.10.1016/j.neuroimage.2011.11.006
8. Basser, P.J. and C. Pierpaoli, *Microstructural and physiological features of tissues elucidated by quantitative-diffusion-tensor MRI.* Journal of magnetic resonance, 2011. **213**(2): p. 560-570
9. Jones, D.K., *Diffusion mri*. 2010: Oxford University Press.
10. Kroenke, C.D., *Using diffusion anisotropy to study cerebral cortical gray matter development.* Journal of Magnetic Resonance, 2018
11. Vrenken, H., P.J. Pouwels, J.J. Geurts, D.L. Knol, C.H. Polman, F. Barkhof, and J.A. Castelijns, *Altered diffusion tensor in multiple sclerosis normal appearing brain tissue: Cortical diffusion changes seem related to clinical deterioration.* Journal of Magnetic Resonance Imaging, 2006. **23**(5): p. 628-636
12. Parker, T.D., C.F. Slattery, J. Zhang, J.M. Nicholas, R.W. Paterson, A.J. Foulkes, I.B. Malone, D.L. Thomas, M. Modat, and D.M. Cash, *Cortical microstructure in young onset Alzheimer's disease using neurite orientation dispersion and density imaging.* Human brain mapping, 2018
13. Masliah, E., R.D. Terry, R.M. DeTeresa, and L.A. Hansen, *Immunohistochemical quantification of the synapse-related protein synaptophysin in Alzheimer disease*. Neuroscience letters, 1989. **103**(2): p. 234-239
14. Terry, R.D., E. Masliah, D.P. Salmon, N. Butters, R. DeTeresa, R. Hill, L.A. Hansen, and R. Katzman, *Physical basis of cognitive alterations in Alzheimer's disease: synapse loss is the major correlate of cognitive impairment.* Annals of neurology, 1991. **30**(4): p. 572-580
15. Scheff, S.W. and D.A. Price, *Synapse loss in the temporal lobe in Alzheimer's disease.* Annals of neurology, 1993. **33**(2): p. 190-199
16. Davies, C., D. Mann, P. Sumpter, and P. Yates, *A quantitative morphometric analysis of the neuronal and synaptic content of the frontal and temporal cortex in patients with Alzheimer's disease*. Journal of the neurological sciences, 1987. **78**(2): p. 151-164

17. Hyman, B.T., G.W. Van Hoesen, A.R. Damasio, and C.L. Barnes, *Alzheimer's disease: cell-specific pathology isolates the hippocampal formation.* Science, 1984. **225**(4667): p. 1168-1170
18. Braak, H. and E. Braak, *Neuropathological stageing of Alzheimer-related changes.* Acta neuropathologica, 1991. **82**(4): p. 239-259
19. Ganepola, T., Z. Nagy, A. Ghosh, T. Papadopoulo, D.C. Alexander, and M.I. Sereno, *Using diffusion MRI to discriminate areas of cortical grey matter.* NeuroImage, 2017
20. Brodmann, K., *Vergleichende Lokalisationslehre der Grosshirnrinde in ihren Prinzipien dargestellt auf Grund des Zellenbaues*. 1909: Barth.
21. Bastiani, M., A.-M. Oros-Peusquens, A. Seehaus, D. Brenner, K. Möllenhoff, A. Celik, J. Felder, H. Bratzke, N.J. Shah, and R. Galuske, *Automatic segmentation of human cortical layer-complexes and architectural areas using ex vivo diffusion MRI and its validation.* Frontiers in neuroscience, 2016. **10**: p. 487
22. Braitenberg, V. and A. Schüz, *Density of Axons*, in *Anatomy of the Cortex*, V. Braitenberg and A. Schüz, Editors. 1991, Springer Berlin Heidelberg: Berlin, Heidelberg. p. 41-45.
23. Jönsson, S.A., A. Luts, N. Guldberg-Kjaer, and R. Öhman, *Pyramidal neuron size in the hippocampus of schizophrenics correlates with total cell count and degree of cell disarray.* European archives of psychiatry and clinical neuroscience, 1999. **249**(4): p. 169-173
24. Cotter, D., D. Mackay, S. Landau, R. Kerwin, and I. Everall, *Reduced glial cell density and neuronal size in the anterior cingulate cortex in major depressive disorder.* Arch Gen Psychiatry, 2001. **58**(6): p. 545-53.10.1001/archpsyc.58.6.545
25. Rajkowska, G., L.D. Selemon, and P.S. Goldman-Rakic, *Neuronal and glial somal size in the prefrontal cortex: a postmortem morphometric study of schizophrenia and Huntington disease.* Archives of general psychiatry, 1998. **55**(3): p. 215-224
26. Maier, S.E. and R.V. Mulkern, *Biexponential analysis of diffusion-related signal decay in normal human cortical and deep gray matter.* Magnetic resonance imaging, 2008. **26**(7): p. 897-904
27. Zhang, H., T. Schneider, C.A. Wheeler-Kingshott, and D.C. Alexander, *NODDI: practical in vivo neurite orientation dispersion and density imaging of the human brain.* Neuroimage, 2012. **61**(4): p. 1000-1016
28. Fukutomi, H., M.F. Glasser, H. Zhang, J.A. Autio, T.S. Coalson, T. Okada, K. Togashi, D.C. Van Essen, and T. Hayashi, *Neurite imaging reveals microstructural variations in human cerebral cortical gray matter.* NeuroImage, 2018
29. Beaujoin, J., C. Destrieux, F. Poupon, I. Zemmoura, J. Mangin, and C. Poupon. *Post-mortem mapping of cortical layers using combined multicompartmental relaxometry and diffusometry at ultra-high field (7T and 11.7T).* in *Proc. Intl. Soc. Mag. Reson. Med.* . 2018.
30. Rocca, M., A. Ceccarelli, A. Falini, P. Tortorella, B. Colombo, E. Pagani, G. Comi, G. Scotti, and M. Filippi, *Diffusion tensor magnetic resonance imaging at 3.0 tesla shows subtle cerebral grey matter abnormalities in patients with migraine.* Journal of Neurology, Neurosurgery & Psychiatry, 2006. **77**(5): p. 686-689
31. Van Cauter, S., J. Veraart, J. Sijbers, R.R. Peeters, U. Himmelreich, F. De Keyzer, S.W. Van Gool, F. Van Calenbergh, S. De Vleeschouwer, and W. Van Hecke, *Gliomas: diffusion kurtosis MR imaging in grading.* Radiology, 2012. **263**(2): p. 492-501
32. Fox, R.J., K. Sakaie, J.-C. Lee, J. Debbins, Y. Liu, D. Arnold, E. Melhem, C. Smith, M. Philips, and M. Lowe, *A validation study of multicenter diffusion tensor imaging:*

reliability of fractional anisotropy and diffusivity values. American Journal of Neuroradiology, 2012. **33**(4): p. 695-700
33. Gilani, N., P. Malcolm, and G. Johnson, *An improved model for prostate diffusion incorporating the results of Monte Carlo simulations of diffusion in the cellular compartment.* NMR Biomed, 2017. **30**(12): p. e3782.10.1002/nbm.3782
34. Reimer, L., *Scanning electron microscopy: physics of image formation and microanalysis*. Vol. 45. 2013: Springer.
35. Stephens, D.J. and V.J. Allan, *Light microscopy techniques for live cell imaging.* Science, 2003. **300**(5616): p. 82-86
36. Denk, W., J.H. Strickler, and W.W. Webb, *Two-photon laser scanning fluorescence microscopy.* Science, 1990. **248**(4951): p. 73-76
37. Sengupta, S., F.J. Fritz, R.L. Harms, S. Hildebrand, D.H.Y. Tse, B.A. Poser, R. Goebel, and A. Roebroeck, *High resolution anatomical and quantitative MRI of the entire human occipital lobe ex vivo at 9.4T.* Neuroimage, 2018. **168**: p. 162-171.10.1016/j.neuroimage.2017.03.039
38. Gilani, N., P. Malcolm, and G. Johnson, *A model describing diffusion in prostate cancer.* Magn Reson Med, 2017. **78**(1): p. 316-326.10.1002/mrm.26340
39. Roebroeck, A., K.L. Miller, and M. Aggarwal, *Ex vivo diffusion MRI of the human brain: Technical challenges and recent advances.* NMR Biomed, 201810.1002/nbm.3941: p. e3941.10.1002/nbm.3941
40. Fieremans, E., D.S. Novikov, J.H. Jensen, and J.A. Helpern, *Monte Carlo study of a two□compartment exchange model of diffusion.* NMR in Biomedicine, 2010. **23**(7): p. 711-724
41. De Santis, S., D.K. Jones, and A. Roebroeck, *Including diffusion time dependence in the extra-axonal space improves in vivo estimates of axonal diameter and density in human white matter.* Neuroimage, 2016. **130**: p. 91-103.10.1016/j.neuroimage.2016.01.047
42. Lee, C.-Y., K.M. Bennett, and J.P. Debbins, *Sensitivities of statistical distribution model and diffusion kurtosis model in varying microstructural environments: a Monte Carlo study.* Journal of Magnetic Resonance, 2013. **230**: p. 19-26
43. Gilani, N., P. Malcolm, and G. Johnson, *A monte carlo study of restricted diffusion: Implications for diffusion MRI of prostate cancer.* Magn Reson Med, 2017. **77**(4): p. 1671-1677.10.1002/mrm.26230
44. Storås, T.H., K.-I. Gjesdal, Ø.B. Gadmar, J.T. Geitung, and N.-E. Kløw, *Prostate magnetic resonance imaging: Multiexponential T2 decay in prostate tissue.* Journal of Magnetic Resonance Imaging, 2008. **28**(5): p. 1166-1172.10.1002/jmri.21534
45. Azevedo, F.A., L.R. Carvalho, L.T. Grinberg, J.M. Farfel, R.E. Ferretti, R.E. Leite, R. Lent, and S. Herculano□Houzel, *Equal numbers of neuronal and nonneuronal cells make the human brain an isometrically scaled□up primate brain.* Journal of Comparative Neurology, 2009. **513**(5): p. 532-541
46. Lauwers, F., F. Cassot, V. Lauwers-Cances, P. Puwanarajah, and H. Duvernoy, *Morphometry of the human cerebral cortex microcirculation: general characteristics and space-related profiles.* Neuroimage, 2008. **39**(3): p. 936-948
47. Herculano□Houzel, S., *The glia/neuron ratio: how it varies uniformly across brain structures and species and what that means for brain physiology and evolution.* Glia, 2014. **62**(9): p. 1377-1391
48. Hawkins, A. and J. Olszewski, *Glia/nerve cell index for cortex of the whale.* Science, 1957. **126**(3263): p. 76-7

49. Codd, S.L. and P.T. Callaghan, *Spin echo analysis of restricted diffusion under generalized gradient waveforms: planar, cylindrical, and spherical pores with wall relaxivity.* Journal of Magnetic Resonance, 1999. **137**(2): p. 358-372
50. Johns, P., *Neurons and glial cells*, in *Clinical Neuroscience*. 2014, Churchill Livingstone. p. 61-69.
51. Abbass, M., K. Trought, D. Long, A. Semechko, and A.H. Wong, *Automated immunohistochemical method to analyze large areas of the human cortex.* Journal of neuroscience methods, 2018. **294**: p. 81-90
52. Liewald, D., R. Miller, N. Logothetis, H.J. Wagner, and A. Schuz, *Distribution of axon diameters in cortical white matter: an electron-microscopic study on three human brains and a macaque.* Biol Cybern, 2014. **108**(5): p. 541-57.10.1007/s00422-014-0626-2
53. Liu, X.B. and C.M. Schumann, *Optimization of electron microscopy for human brains with long-term fixation and fixed-frozen sections.* Acta Neuropathol Commun, 2014. **2**(1): p. 42.10.1186/2051-5960-2-42
54. Zikopoulos, B. and H. Barbas, *Changes in prefrontal axons may disrupt the network in autism.* Journal of Neuroscience, 2010. **30**(44): p. 14595-14609
55. Deitcher, Y., G. Eyal, L. Kanari, M.B. Verhoog, G.A. Atenekeng Kahou, H.D. Mansvelder, C.P. De Kock, and I. Segev, *Comprehensive Morpho-Electrotonic Analysis Shows 2 Distinct Classes of L2 and L3 Pyramidal Neurons in Human Temporal Cortex.* Cerebral Cortex, 2017. **27**(11): p. 5398-5414
56. Hildebrand, S., A. Schueth, A. Herrler, R. Galuske, and A. Roebroeck, *Scalable cytoarchitectonic characterization of large intact human neocortex samples.* bioRxiv, 2018: p. 274985
57. Iglesias, J.E., M. Modat, L. Peter, A. Stevens, R. Annunziata, T. Vercauteren, E. Lein, B. Fischl, and S. Ourselin, *Joint registration and synthesis using a probabilistic model for alignment of MRI and histological sections.* arXiv preprint arXiv:1801.05284, 2018
58. Petrov, Y., *Ellipsoid fit.* MATLAB Central File Exchange, 2009: p. 24693
59. Jensen, J.H. and J.A. Helpern, *MRI Quantification of Non-Gaussian Water Diffusion by Kurtosis Analysis.* NMR in biomedicine, 2010. **23**(7): p. 698-710.10.1002/nbm.1518
60. Jensen, J.H., J.A. Helpern, A. Ramani, H. Lu, and K. Kaczynski, *Diffusional kurtosis imaging: the quantification of non-gaussian water diffusion by means of magnetic resonance imaging.* Magn Reson Med, 2005. **53**(6): p. 1432-40
61. Thue, A., *Über die dichteste Zusammenstellung von kongruenten Kreisen in einer Ebene, von Axel Thue*. 1910: J. Dybwad.
62. Pagani, E., J.G. Hirsch, P.J. Pouwels, M.A. Horsfield, E. Perego, A. Gass, S.D. Roosendaal, F. Barkhof, F. Agosta, and M. Rovaris, *Intercenter differences in diffusion tensor MRI acquisition.* Journal of Magnetic Resonance Imaging, 2010. **31**(6): p. 1458-1468
63. Palombo, M., D.C. Alexander, and H. Zhang, *A generative model of realistic brain cells with application to numerical simulation of diffusion-weighted MR signal.* arXiv preprint arXiv:1806.07125, 2018
64. Sousa, D., F. Borlinhas, and H. Ferreira, *Estimation of breast tumour tissue diffusion parameters from histological images and Monte-Carlo simulations.* Soc. Mag. Reson. Med., 2016. **24**: p. 2474.10.13140/RG.2.2.32262.06726
65. Gilani, N. and G. Johnson, *Bias in MRI Measurements of Apparent Diffusion Coefficient and Kurtosis: Implications for Choice of Maximum Diffusion Encoding.* Applied Magnetic Resonance, 2018: p. 1-15

66. Gilani, N., P.N. Malcolm, and G. Johnson, *Parameter Estimation Error Dependency on the Acquisition Protocol in Diffusion Kurtosis Imaging.* Appl Magn Reson, 2016. **47**(11): p. 1229-1238.10.1007/s00723-016-0829-x
67. Palombo, M., N. Shemesh, A. Ianus, D. Alexander, and H. Zhang. *Abundance of cell bodies can explain the stick model's failure in grey matter at high b-value*. in *Proc. Intl. Soc. Mag. Reson. Med.* . 2018.
68. Kärger, J., *NMR self-diffusion studies in heterogeneous systems.* Advances in Colloid and Interface Science, 1985. **23**: p. 129-148
69. Chuhutin, A., B. Hansen, and S.N. Jespersen, *Precision and accuracy of diffusion kurtosis estimation and the influence of b□value selection.* NMR in Biomedicine, 2017. **30**(11)
70. Novikov, D.S., V.G. Kiselev, and S.N. Jespersen, *On modeling.* Magn Reson Med, 2018. **79**(6): p. 3172-3193.10.1002/mrm.27101
71. Veraart, J., E. Fieremans, U. Rudrapatna, D.K. Jones, and D.S. Novikov, *Biophysical modeling of the gray matter: does the "stick" model hold?* Soc. Mag. Reson. Med. , 2018: p. 1094
72. Baron, C.A. and C. Beaulieu, *Oscillating gradient spin-echo (OGSE) diffusion tensor imaging of the human brain.* Magn Reson Med, 2014. **72**(3): p. 726-36.10.1002/mrm.24987
73. Clark, C.A., M. Hedehus, and M.E. Moseley, *Diffusion time dependence of the apparent diffusion tensor in healthy human brain and white matter disease.* Magnetic resonance in medicine, 2001. **45**(6): p. 1126-1129
74. Jones, D.K., T.R. Knösche, and R. Turner, *White matter integrity, fiber count, and other fallacies: the do's and don'ts of diffusion MRI.* Neuroimage, 2013. **73**: p. 239-254
75. Assaf, Y., *Imaging laminar structures in the gray matter with diffusion MRI.* NeuroImage, 2018
76. Aggarwal, M., D.W. Nauen, J.C. Troncoso, and S. Mori, *Probing region-specific microstructure of human cortical areas using high angular and spatial resolution diffusion MRI.* Neuroimage, 2015. **105**: p. 198-207.10.1016/j.neuroimage.2014.10.053
77. Cottaar, M., M. Bastiani, C. Chen, K. Dikranian, D. Van Essen, T.E. Behrens, S.N. Sotiropoulos, and S. Jbabdi, *A gyral coordinate system predictive of fibre orientations.* NeuroImage, 2018. **176**: p. 417-430
78. Bouhrara, M. and R.G. Spencer, *Fisher information and Cramér-Rao lower bound for experimental design in parallel imaging.* Magnetic Resonance in Medicine, 2018. **79**(6): p. 3249-3255.doi:10.1002/mrm.26984
79. Gilani, N., A.B. Rosenkrantz, P. Malcolm, and G. Johnson, *Minimization of errors in biexponential T2 measurements of the prostate.* J Magn Reson Imaging, 2015. **42**(4): p. 1072-7.10.1002/jmri.24870
80. Lemberskiy, G., E. Fieremans, J. Veraart, F.M. Deng, A.B. Rosenkrantz, and D.S. Novikov, *Characterization of prostate microstructure using water diffusion and NMR relaxation.* Front Phys, 2018. **6**: p. 91.10.3389/fphy.2018.00091
81. Cao, Y., Y. Zhang, Y. Wang, W. Liu, and D. Han, *Improved stimulated echo in diffusion magnetic resonance imaging: introducing a pi pulse for SNR enhancement.* Magn Reson Med, 2019. **81**(5): p. 2905-2914.10.1002/mrm.27653
82. Nguyen, K.-V., E. Hernández-Garzón, and J. Valette, *Efficient GPU-based Monte-Carlo simulation of diffusion in real astrocytes reconstructed from confocal microscopy.* Journal of Magnetic Resonance, 2018. **296**: p. 188-199

Table 1. Diffusion weighted measurements of the cortex from the literature.

Study	Tissue type	Scanner(s)	*b*-values /smm^{-2}	Other details	ADC /μm^{2}ms^{-1}	K
Rocca et al. [30]	Gray matter	3 T Intera Philips	0, 1000 32 directions	T_E=80 Fat suppression	1.00 (±0.05)	-
Rocca et al. [30]	White matter	3 T Intera Philips	0, 1000 32 directions	T_E=80 Fat suppression	0.79 (±0.07)	-
Van Cauter et al. [31]	Gray matter	3 T Achieva Philips	0, 700, 1000, 2800 25, 40, 75 directions, respectively	Δ= 48, δ=20 T_E=90	0.99 (0.93-1.06)	0.85 (0.80-0.87)
Van Cauter et al. [31]	White matter	3 T Achieva Philips	0, 700, 1000, 2800 25, 40, 75 directions, respectively	Δ= 48, δ=20 T_E=90	1.03 (0.65-1.12)	0.86 (0.76-0.93)
Fox et al. [32]	Deep gray matter	3 T Trio Siemens, 3 T Signa GE	0, 1000 33 directions	T_E=94, or 100	Around 0.7 (±0.1)	-
Fox et al. [32]	Cortical gray matter	3 T Trio Siemens, 3 T Signa GE	0, 1000 33 directions	T_E=94, or 100	Around 1.15 (±0.3)	-
Fox et al. [32]	Deep white matter	3 T Trio Siemens, 3 T Signa GE	0, 1000 33 directions	T_E=94, or 100	Around 0.75 (±0.2)	
MC simulations*	LII, LIII (Neuron and glia only)	-	0-2500 (15 equally distanced *b*-values), 18 directions	T_{TD}=40-100 ms Mathematically reconstructed geometry	1.08 (0.77-1.38)	0.60 (0.34-1.04)
MC simulations*	LII, LIII (Neuron and glia only)	-	0-2500 (15 equally distanced *b*-values), 18 directions	T_{TD}=40-100 ms Geometry from Microscopy	1.25 (1.20-1.30)	0.14(0.10-0.18)
MC simulations	LIV, LV (Neuron, glia, axon)	-	0-2500 (15 equally distanced *b*-values), 18 directions	T_{TD}=40-100 ms Mathematically reconstructed geometry	1.05 (0.87-1.46)	0.66 (0.26-0.84)
MC simulations*	Deep white matter (Axon only)	-	0-2500 (15 equally distanced *b*-values), 18 directions	T_{TD}=40-100 ms Mathematically reconstructed geometry	0.85 (0.75-1.01)	0.95(0.84-1.05)

*The simulations were performed for all of the cell diameters and densities mentioned in the text.

(a)

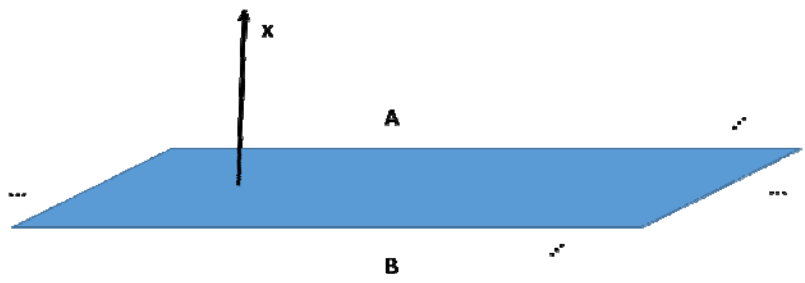

(b)

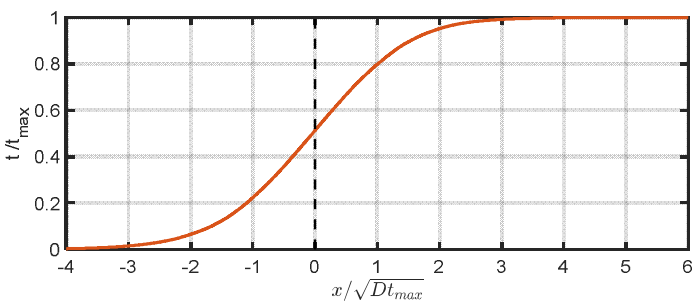

(c)

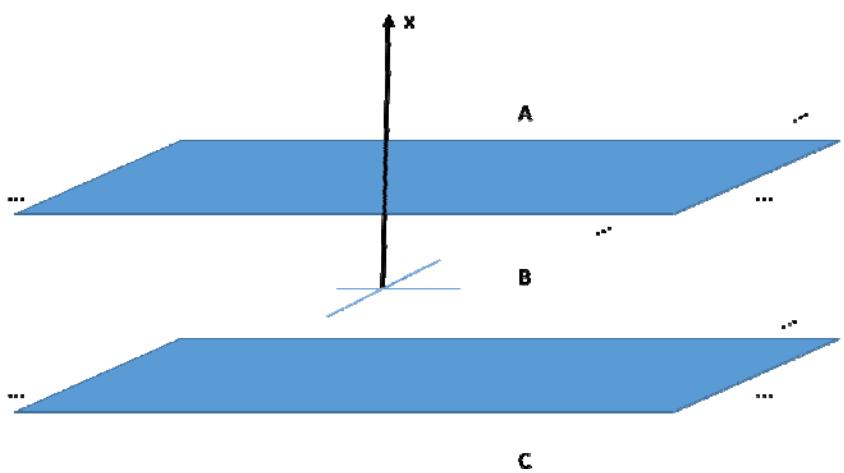

(d)

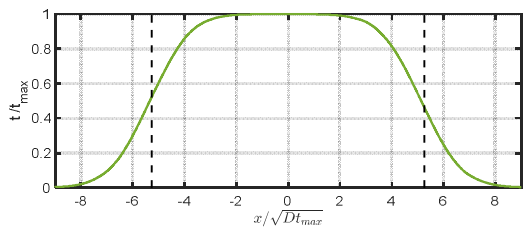

(e)

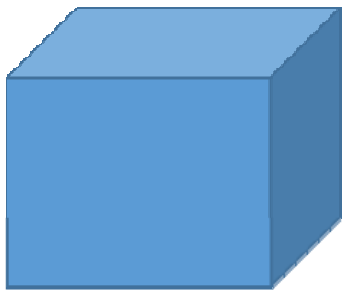

(f)

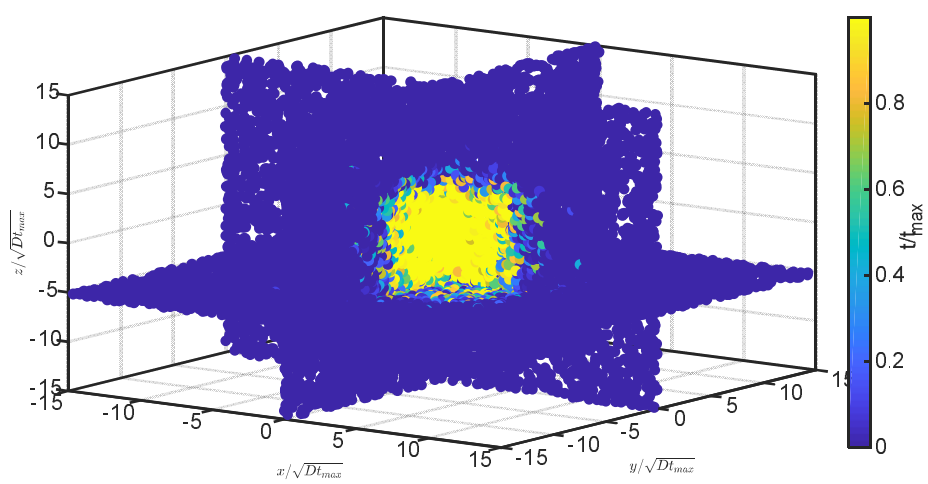

Fig. 1 Residence time simulations in two mediums (WM and GM) separated by one plate (a) and (b), three mediums (cortical layers) separated by two plates (c) and (d), and inside a voxel (e) and (f). Notes: the dashed lines in (b) and (d) are x of the planes. For (b-f) all of the plates were either located at -5.27 or 5.27 $/(Dt_{\max})^{0.5}$.

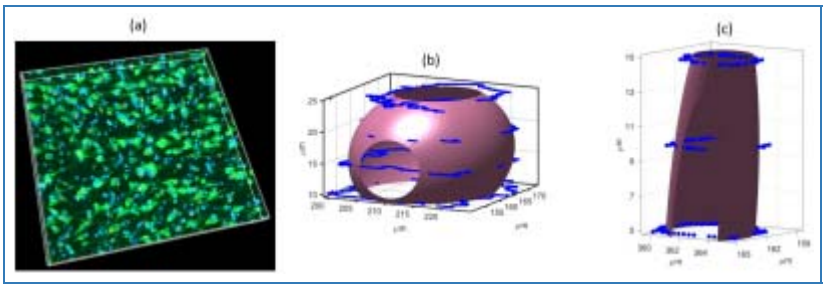

Fig. 2 A 3D rendering of the 3D microscopy volume, with nucleus label in blue and cytoplasmic cell body label in green (a). Segmented areas of a neuron (b) and a glia (c) and the ellipsoids fitted to them. On average neurons were best described by spheres with radii of 12.0±4.6 and glia by ellipsoids with axes 2.73±0.63, 2.73±0.63, 8.98±1.77 µm in the visual cortex with N=50. Note: resolution and slice thickness of microscopy were 0.36×0.36 µm2, and 4.98 µm, respectively.

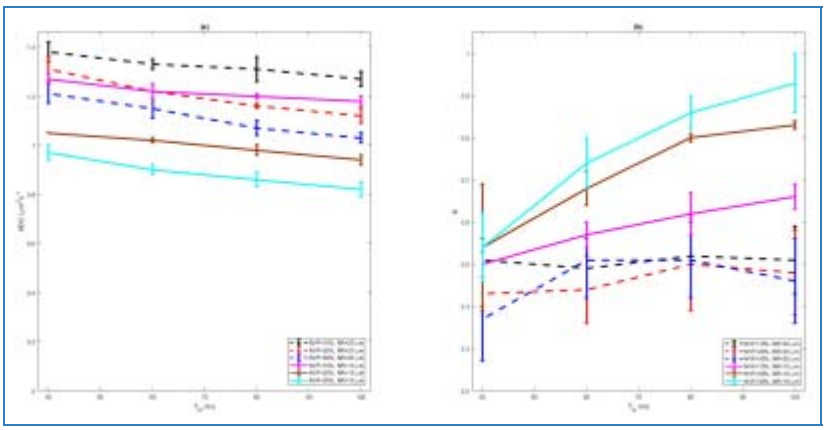

Fig. 3 ADC (a) and kurtosis (b) of the simulated neuronal/glial mixture with variable neuron volume fractions (NVF) and neuron radii (NR), for constant glial volume fraction, for diffusion times of 40-100 ms, with the indirect (first) simulation method. Glial sizes were the same as Fig. 1 and their volume fraction was 0.03-0.07.

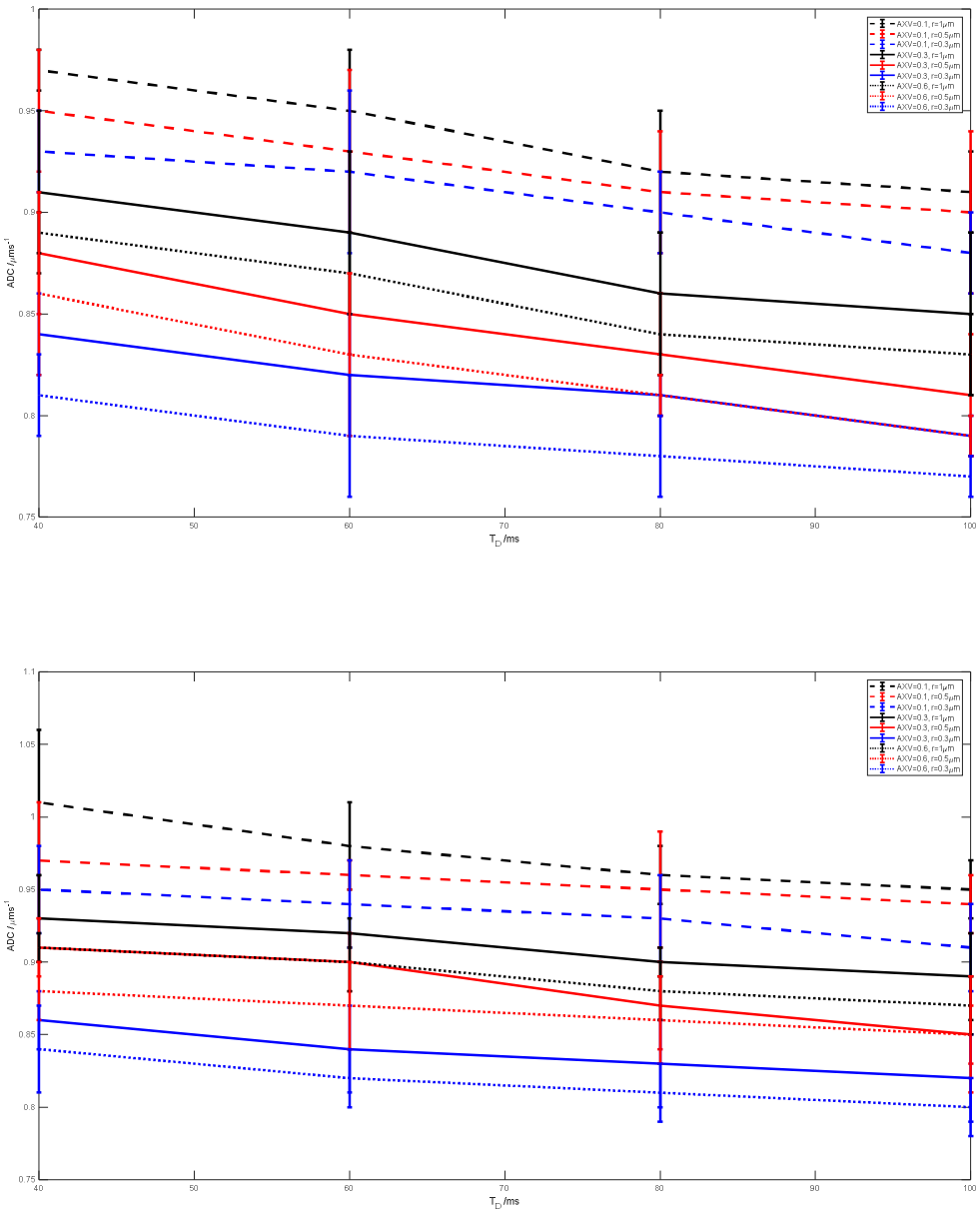

Fig. 4 ADC simulated myelinated (a) and unmyelinated (b) axons with variable axonal volume fractions (AXV) and axon radii (r), in absence of cell bodies, for diffusion times of 40-100 ms, with the indirect (first) simulation method.

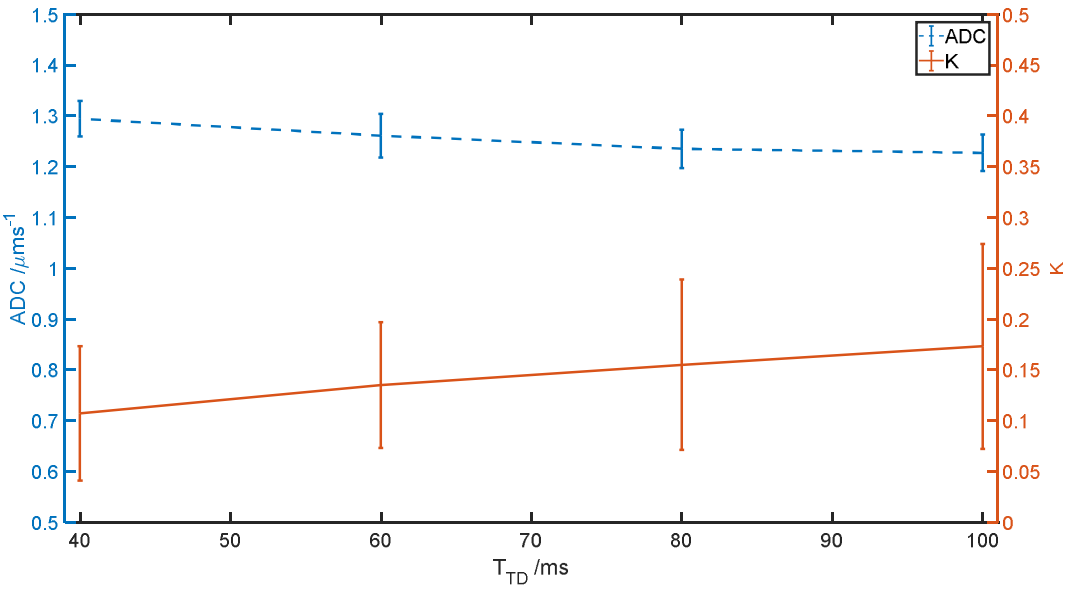

Fig. 5 Direct simulation of (a) ADC and (b) *K* in a TPM microscopy sample of the visual cortex.